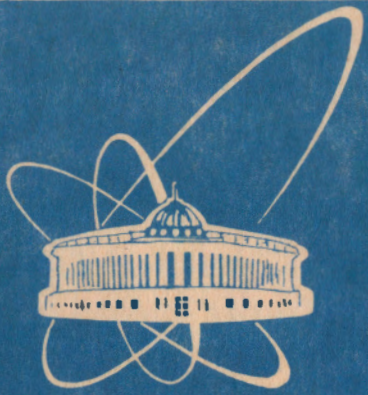

ОБЪЕДИНЕННЫЙ
ИНСТИТУТ
ЯДЕРНЫХ
ИССЛЕДОВАНИЙ

Дубна

E10-95-318

M.P.Bussa[1], L.Fava[1], L.Ferrero[1], A.Grasso[1], V.V.Ivanov,
I.V.Kisel, E.V.Konotopskaya, G.B.Pontecorvo

ON A POSSIBLE SECOND-LEVEL TRIGGER FOR THE EXPERIMENT **DISTO**

Submitted to «Nuovo Cimento»

[1]INFN Sezione di Torino, Torino, Italy

1995

Бусса М.П. и др.
E10-95-318

Возможный триггер второго уровня для эксперимента DISTO

В эксперименте DISTO для подавления фона и для эффективного отбора событий с короткоживущими Λ-, Σ- и φ-частицами будет использован двухуровневый триггер. Триггер первого уровня будет применен для отбора событий по множественности. Триггер второго уровня будет служить для распознавания треков, для поиска вторичной вершины, а также для идентификации зарегистрированных частиц.

Работа выполнена в Лаборатории вычислительной техники и автоматизации и Лаборатории ядерных проблем ОИЯИ.

Препринт Объединенного института ядерных исследований. Дубна, 1995

Bussa M.P. et al.
E10-95-318

On a Possible Second-Level Trigger for the Experiment DISTO

A two-level trigger is to be applied for suppression of the background and for effective selection of events involving short-lived Λ-, Σ- and φ-particles in the experiment DISTO. The first-level trigger is intended for selection of events by their multiplicity. The second-level trigger is applied for track recognition, in searching for a secondary vertex, and for identifying the detected particles.

The investigation has been performed at the Laboratory of Computing Techniques and Automation and at the Laboratory of Nuclear Problems, JINR.

Preprint of the Joint Institute for Nuclear Research. Dubna, 1995

1. Introduction

At present, an experiment is being prepared by the DISTO (**D**ubna – **I**ndiana – **S**aclay – **TO**rino) [1] collaboration for studying spin effects in the reaction

$$\uparrow pp \longrightarrow pK^+Y$$

with the polarized proton beam of Saturne (Saclay, France). The aim is to carry out a detailed study of the reactions $pp \longrightarrow pK^+\Lambda^0$, $pp \longrightarrow pK^+\Sigma^0$ and $pp \longrightarrow pp\phi^0$.

The layout of the DISTO experiment is presented in Figure 1. The DISTO spectrometer has a cylindrical geometry and consists of two arms situated symmetrically about the beam direction. In each arm there are 5 detectors: 2 scintillation fibre chambers, 2 multiwire proportional chambers (MWPC) and an outer detector, which consists of 2 planes, vertical and horizontal, of scintillation hodoscope counters. At present, the possibility of placing Cherenkov counters behind the scintillation hodoscope is investigated. The detectors cover a scattering angle of 45^0 in the horizontal plane and a dip angle of $\pm 20^0$. The detectors and the liquid-hydrogen target are situated in the magnetic field, which is perpendicular to the incident beam.

A two-level trigger [2] is to be applied for suppression of the background and for effective selection of useful events in the presence of a dominant background, mainly due to $pp \longrightarrow pp\pi^+\pi^-$ events. The first-level trigger is intended for selection of events by their multiplicity: only four-prong events are selected. Events accepted by the first-level trigger are then examined with the help of the second-level trigger.

In this paper a possible second-level trigger, to be realized on the basis of four RISC-processors and consequently applied for track recognition, in searching for a secondary vertex, and for identifying the detected particles, is presented.

2. Track recognition with the help of a cellular automaton

For track recognition the coordinate information arriving from the scintillation fibre chambers and from the multiwire proportional chambers[1] is taken into account. Only coordinates corresponding to the vertical plane are used. This is due to the influence of the magnetic field on the charged particle trajectories in this projection being negligible and to the possibility of approximating tracks by straight lines and thus speeding up their reconstruction. The actual track recognition is done applying the cellular automaton [3].

Schematically, a cellular automaton may be visualized as a regular spatial net; each cell of which is capable of assuming a number of discrete states. Time is varied in discrete steps, and evolution of the system obeys certain a priori fixed rules determining the new state of each individual cell at each successive step in accordance with the states of its nearest neighbours [4, 5].

A typical cellular automaton is constructed in accordance with the following algorithm:

1. cells and their possible discrete states are defined; usually, each cell may assume one of two states, 0 or 1; however, there may be cellular automata with more states;

2. interconnections between cells are defined; usually, each cell can only communicate with neighbour cells;

3. rules determining evolution of the cellular automaton are fixed; they depend on the actual problem considered and usually have a simple functional form;

4. the cellular automaton is a timed system, in which all cells change states simultaneously.

In our case, a cell is identified with the straight-line segment connecting two hits in neighbouring detectors. To take into account the inefficiency of the coordinate chambers one must consider, also, the segments connecting hits skipping one chamber. At each step a cell can assume one of two possible states: 1, if the segment can be considered a part of the track, and 0 otherwise. Clearly, only such segments can be considered neighbours, which have a common point serving as the end of one segment and the beginning of the second.

Taking into account the geometry of the spectrometer DISTO, it is convenient to utilize a cylindrical coordinate system and to conduct track recognition in the vertical ROZ plane, where charged particle trajectories can be approximated by straight lines. Here, the OR axis coincides with the radius and the OZ axis is perpendicular to the beam.

In establishing the criterion for assigning segments to a track it is convenient to use the angle φ between two adjacent segments. Owing to the coordinate detectors having a discrete structure and to multiple scattering in the material of the experimental apparatus, the angles between track segments in the real experiment are not zero, but an upper limit can be imposed.

In Figure 2 the distribution of the angles φ for tracks simulated with the aid of the LACYL code[2] is presented. From the Figure it follows that for most of the tracks the angles φ satisfy the inequality $|\varphi| \leq 2.0^0$; this value can be used as a criterion for the selection of useful segments. It must be noted, here, that a notable part of particles are scattered in the coordinate chambers through large angles, which hinders their recognition. Figure 3 shows the distribution of tracks over the maximum angle φ for each individual track.

Upon completion of the work of the cellular automaton additional testing of the quality of reconstructed tracks (for instance, for the presence of at least two hits belonging only to each individual track) is carried out. This permits rejecting "phantom" tracks, which were accidentally constructed from hits belonging to different tracks.

Figures 4 and 5 present the respective initial and resultant configurations of the cellular automaton for a typical simulated event. One can note the absence of hits in the first chamber and the presence of one noise hit in the third chamber.

In Table 1 the total numbers of generated and reconstructed events are presented versus the number of tracks in the individual events. In all, 1000 events have been simulated. A simple comparison of the figures reveals the high efficiency of the cellular automaton. The difference between the numbers is due to the large-angle scattering of secondary particles that occurs in the coordinate chambers and which may result in the multiplicity of a reconstructed event being wrong.

A detailed analysis of the cellular automaton functioning and examination of the generated events, making use of graphical computer images of the events, has shown that tracks containing large scattering angles φ are lost. Some of such tracks can still be reconstructed, if break happens in the first three chambers and the track has hits in all the chambers. In this case the track is reconstructed using the information from the three chambers. An event containing a track that cannot be fully reconstructed is usually assigned fictitious tracks and may be lost.

An analysis of these situations is presented in the Figure 6, where the upper curve shows the fraction (in %) of lost tracks versus the upper limit chosen for the angle, φ_{max}. Comparison of this Figure with Figure 3 reveals that a certain fraction of tracks with large breaks can actually be recognized. The lower curve shows the contribution (in %) of added, "phantom" tracks. Such tracks are mostly contructed from points belonging to lost tracks.

Figure 7 shows the efficiency of event reconstruction versus the upper limit for the angle φ_{max}. The maximum efficiency of event reconstruction is achieved at $|\varphi_{max}| = 2.5^0$. It equals 79 % and represents the limit value, determined by the fraction of tracks with large breaks: approximately 18 % of the events contain such broken tracks, given this boundary angle.

3. Identifying the secondary vertex

The production kinematics of an unstable particle gives rise to a certain pecu-

[1] The coordinate detectors are located at 20 cm, 40 cm, 90 cm and 120 cm from the center of the target, respectively.

[2] For simulating the physical processes and operation of the experimental apparatus a computer program termed LACYL based on the GEANT package [6] has been developed.

liarity in the event geometry. It consists in the momenta of the unstable particle decay products being mainly not directed along the primary beam. This results in the momenta of the secondary particles produced in the decay of the unstable particle having directions differing essentially from those of the particles emitted from the primary vertex. Thus, the idea arose to utilize the coordinate of the intersection point of a straight line (coinciding with the particle track) with the direction of the primary beam as a parameter permitting revelation of the existence of a secondary vertex in the event being considered [7]. To a certain extent this quantity is similar to the impact parameter D, but here, unlike ref. [8], the dispersion of the track about the YOZ-plane (or the XOZ-plane) is to be used as the measure.

The distributions of the Z-coordinates of intersection points of particle trajectories in the YOZ-plane[3] are presented in Figure 8 a for tracks corresponding to the proton p_1 and the K^+ (background events), while the respective distributions for proton p_2 and the π^- from the Λ^0 decay (signal events) are presented in Figure 8 b. They are seen to differ significantly.

By analogy with ref. [8] we shall now pass to the moment variables

$$\xi_{02} = \frac{1}{N}\sum_{i=1}^{N}(D_z - \bar{D}_z)^2 \quad and \quad \xi_{11} = \frac{1}{N}\sum_{i=1}^{N}(\Phi - \bar{\Phi})(D_z - \bar{D}_z),$$

where $\bar{D}_z$ and $\bar{\Phi}$ are the mean values of D_z and Φ (set equal to zero), and N is the number of tracks of the sort considered. As the variable D_z we took the distance from the intersection point of the track with the axis of the beam to the origin of the coordinate system. In Figures 9 a and 9 b the joint distributions of the random variables ξ_{02} and ξ_{11} are presented for practically all the background events and for those signal events (shaded in the Figures) that happened to be in the same region as the background events.

For the chosen critical value of $\xi_{02} = 0.5$ the number of background events interpreted as signal events (error of the second kind) amounted to 37, while the amount of signal events that happened to be among the background events (error of the first kind) equaled 57. The corresponding quantities for the variable ξ_{11} in the range of $|\xi_{11}| \leq 0.1$ were 5 and 126. Now, if a neural network is utilized for classification of events in the space of the variables ξ_{02} and ξ_{11}, then the identification of signal and background events will practically be totally unambiguous.

4. Identifying secondary particles

In all the processes of interest there will be charged K-mesons detected in the final state. Therefore, when the selection of events by multiplicities is completed (at the stage of the I-level trigger) and the technique of cellular automata is applied for revealing the curved tracks in the horizontal plane, it will be necessary to identify the detected particles [9].

To this end we shall first try to reconstruct the momentum of a charged particle by the angle of its deviation in the inhomogeneous magnetic field. The drawing presented in Figure 10 illustrates how the tangent of the deviation angle φ of a charged particle

[3]The influence of the magnetic field on a charged particle is very small in the YOZ-plane, so the trajectories of particles in this projection are almost linear; this makes it more simple to search for them and to determine parameters in the real-time of the experiment.

in the magnetic field is determined from the coordinates of "hits" in the fibre chambers (chambers 1 and 2) and in the MWPC chambers (chambers 3 and 4):

$$\tan\varphi = \frac{k_2 - k_1}{1 + k_1 k_2}, \qquad k_1 = \frac{x_2 - x_1}{z_2 - z_1}; \qquad k_2 = \frac{x_4 - x_3}{z_4 - z_3}.$$

The distribution of random values

$$C_m = \tan\varphi \times P,$$

where P is the momentum of the particle being considered, is presented in Figure 11. From this picture the conclusion can be made that for reconstruction of a great majority of the detected particles (p, $K^\pm$ and $\pi^\pm$) one can actually consider the field to be homogeneous, i.e. the particle momenta may be determined from the following relation:

$$P_c = \frac{\bar{C}_m}{\tan\varphi},$$

where $\bar{C}_m$ is the most probable value of variable C_m. The distribution of random values $\Delta P = P - P_c$ characterizing the reconstruction accuracy of momenta for secondary particles with momenta between 0 and 3 GeV/c is given in Figure 12; the distribution of random values $\frac{\Delta P}{P}$ exhibits a spread amounting to $\approx 5\%$.

Taking advantage of the signal heights from the Cherenkov counter and of the reconstructed momenta of the secondary particles, one can select the events of interest by the presence of $K^\pm$-mesons among the secondaries.

In Figure 13 a two-dimensional distribution of the variables "P vs β" is represented. In the example we use the quantity $\beta = P/E$, where E is the particle energy. The value of β, obtained from the expression presented above is supplemented with an error equal to $\Delta\beta$, generated in accordance with the Gaussian distribution N(0,0.03), which corresponds to an $\approx 5\%$ error[4] for the whole range of β values. From the Figure it can be seen that the secondary p, π^+ and K^+ are quite well separated.

As a non-linear classifier permitting identification of the particle under consideration in the space of the indicated random variables one can utilize a multi-layer neural network of the feedforward type from the JETNET 2.0 package [10]. In Figure 14 the distribution is presented of the output signals from a neural network trained, also, for identification of kaons:

- the empty histogram corresponds to tracks of p and π;
- the dark histogram corresponds to tracks of K^+.

The probability of identifying kaons amounted to 89%. The efficiency of kaon identification may be increased approximately to the level of 95 – 97%, if the particle examined is first tested as a proton and then, alternatively, as a pion or a kaon (the order is irrelevant).

5. Conclusion

A model of a second-level trigger for the spectrometer DISTO has been developed, which is based

[4]Estimation reveals that the experimental error should not exceed this value.

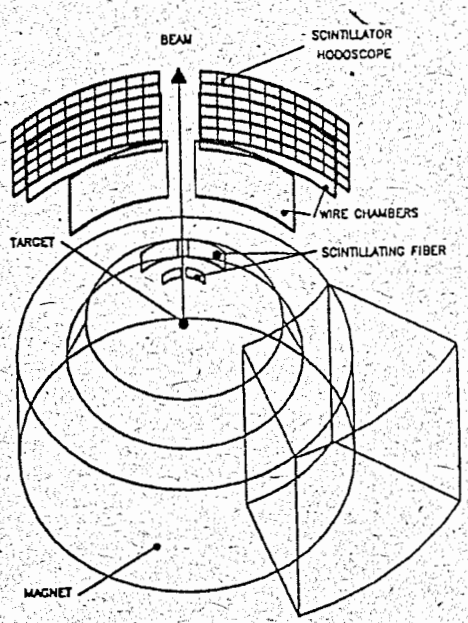

Figure 1: The layout of the DISTO experiment

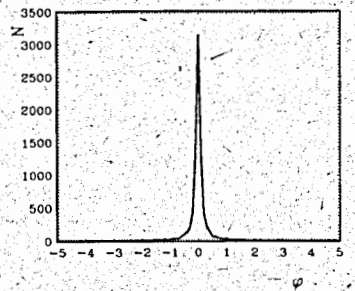

Figure 2: Distribution of angles φ for simulated tracks

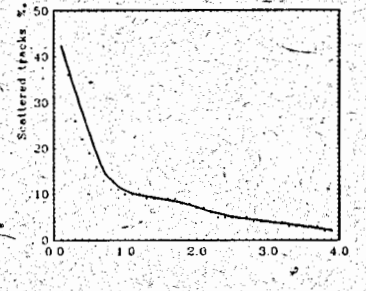

Figure 3: Distribution of tracks over the maximum angle φ in the track

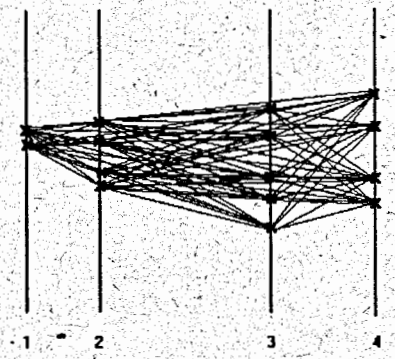

Figure 4: Initial configuration of the cellular automaton for a typical Monte-Carlo event in the spectrometer DISTO

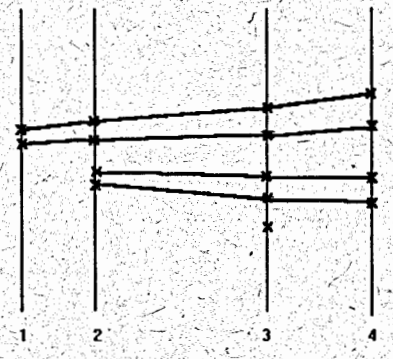

Figure 5: Resultant configuration of the cellular automaton for the event presented in Figure 4

Number of tracks in event	Number of generated events	Number of reconstructed events
1	1	0
2	48	57
3	447	478
4	502	463
5	2	2

Table 1: Distribution of the number of simulated and reconstructed events depending on the number of tracks in the event (the total number of generated events was equal to 1000)

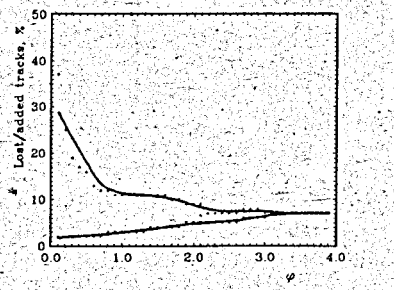

Figure 6: Fraction (in %) of lost (upper curve) and "phantom" (bottom curve) tracks versus boundary angle φ_{max}

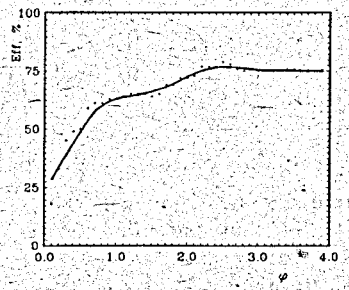

Figure 7: Efficiency of event reconstruction versus boundary angle φ_{max}

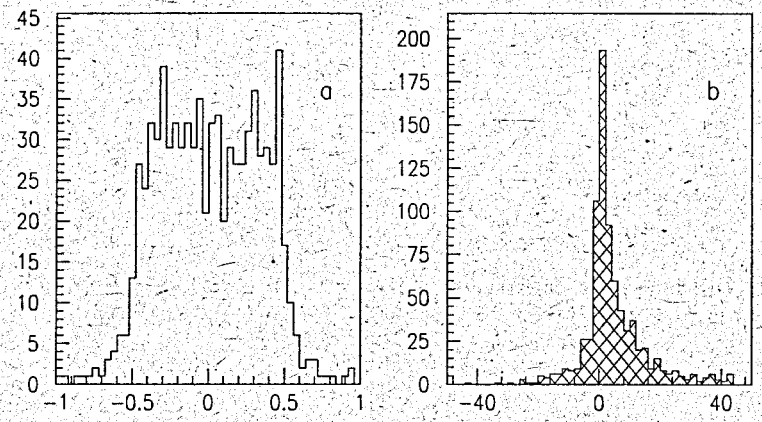

Figure 8: Distributions of the Z-coordinates of intersection points of particle trajectories with the direction of the primary beam in the $Y0Z$-plane for background (a) and signal (b) events

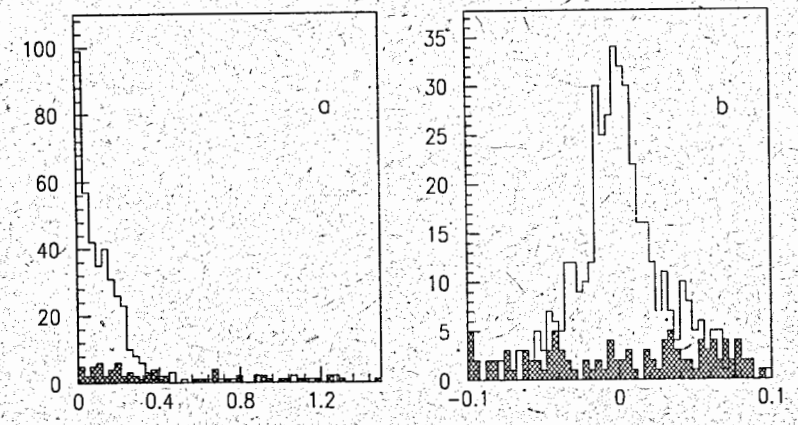

Figure 9: Distributions of the random variables ξ_{02} (a) and ξ_{11} (b) for background events and for those signal events (shaded in the Figures) that happened to be in the same region as the background events

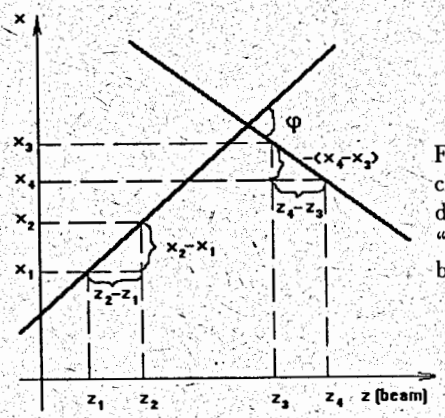

Figure 10: Deviation angle φ of a charged particle in magnetic field determined by the coordinates of "hits" in the fibre and MWPC chambers

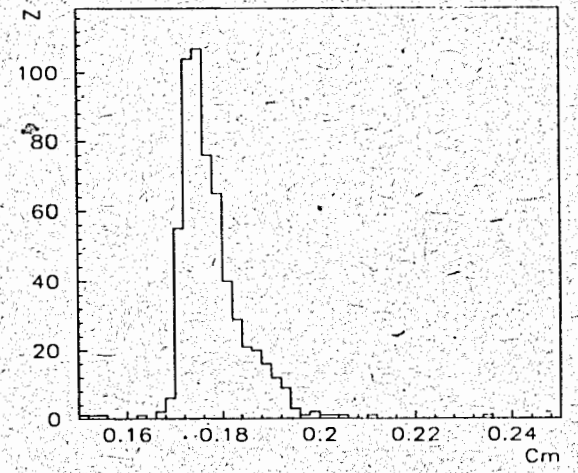

Figure 11: Distribution of random value $C_m = \tan\varphi \times P$ (see text)

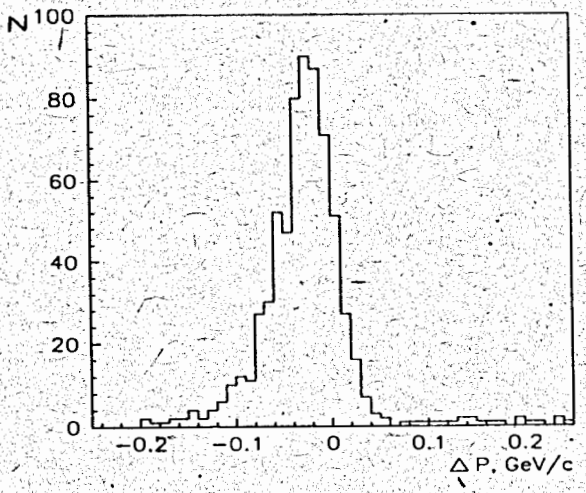

Figure 12: Distribution of random value $\Delta P = P - P_c$ (see text)

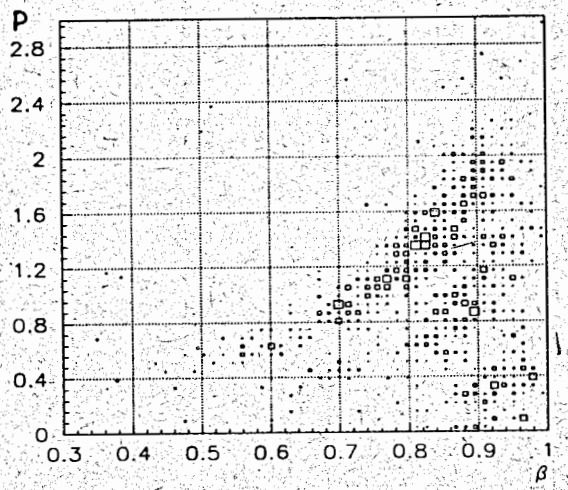

Figure 13: Two-dimensional distribution of variables P *vs* β: $\beta = P/E$, where E is the particle energy

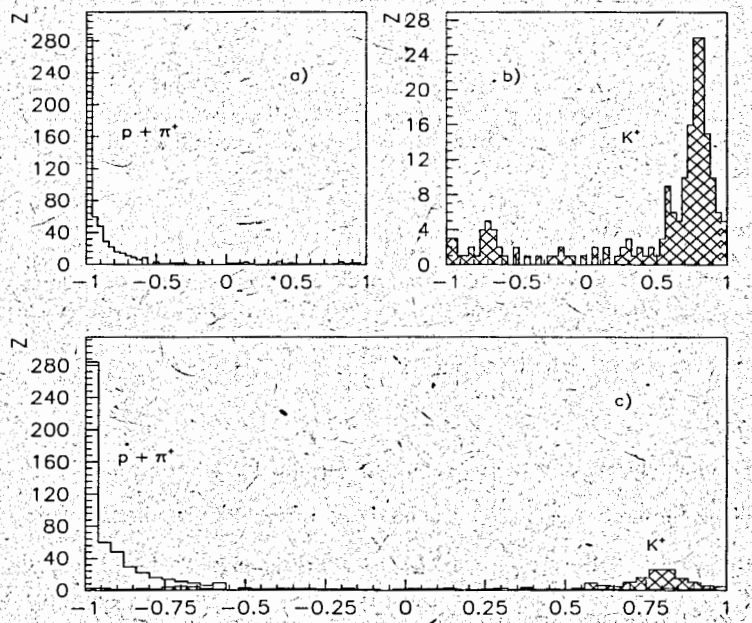

Figure 14: Distributions of output signals from neural network trained for identification of kaons: a) for tracks of p and π; b) for tracks of K^+; c) summary

- on a novel approach for recognition of straight tracks applying the cellular automaton,
- on the new variables permitting effective selection of events containing a secondary vertex,
- and on the identification of the secondary charged particles applying a neural network.

The considered model has shown high efficiency and speed (for simulated events) in recognition of trajectories of detected particles, in their identification and in selection of events containing a secondary vertex. At present this model is being realized on the basis of 4-RISC processors, which are used in the spectrometer DISTO for data acquisition and on-line analysis.

6. Acknowledgements

VVI and IVK acknowledge the Commission of the European Community for partial support within the framework of the EU – RUSSIA Collaboration under the ESPRIT contract P9282-ACTCS.

References

[1] DISTO collaboration, J.Arvieux et al., 1991, Proposal 213 at Saturne.

[2] "DISTO experiment trigger". DISTO meeting, Torino, September 24, 1992.

[3] M.P. Bussa et al.: *"Application of a Cellular Automaton for Recognition of Straight Tracks in the Spectrometer DISTO"*. JINR Preprint, E10-95-32, Dubna, 1995. Submitted to "Mathematical Modelling".

[4] S. Wolfram (ed.): *"Theory and Applications of Cellular Automata"*. World Scientific, 1986.

[5] T. Toffoli and N. Margolus: *"Cellular Automata Machines: A New Environment for Modelling"*. MIT Press, Cambridge, Mass., 1987.

[6] R. Brun et al. *GEANT3 Reference Manual.* CERN Program Library Long Writeup W5013, DD/EE/84-1, 1987.

[7] V.V.Ivanov and G.B.Pontecorvo: *"An Algorithm for Identifying Secondary Vertices"*. In: Proc. of the Third International Workshop on Software Engineering, Artificial Intelligence and Expert Systems for High Energy and Nuclear Physics, Oberammergau, Oberbayern, Germany, October 4–8, 1993; *"New Computing Techniques in Physics Research III"*, Edited by K.-H. Becks & D. Perret-Gallix, "World Scientific", 1994, p. 321–326.

[8] L.Gupta et al.: *"Neural Network Trigger Algorithms for Heavy Quark Event Selection in a Fixed Target High Energy Physics Experiment"*. FERMILAB-Pub-91/17, FNAL, Batavia, 1991.

[9] M.P. Bussa et al.: *"An Algorithm for Identifying Events in the Experiment DISTO"*. JINR Rapid Communications, 2(70)-95, Dubna, 1995.

[10] L. Lönnblad, C. Peterson and T. Rögnvaldsson: *"Pattern Recognition in High-Energy Physics with Artificial Neural Networks: JETNET 2.0"*, Comp. Phys. Commun., **70**, 1992, p.167.

Received by Publishing Department on July 14, 1995.